OverFlight: Graphical Flight Operations Planning

Robert F. Rau
Coherent Applications, Inc
Ann Arbor, MI, USA

Karl Wiedemann
Analytical Services & Materials, Inc
Hampton, VA, USA

William Pogge
Analytical Mechanics Associates
Scottsdale, AZ, USA

James H. Stephenson
U.S. Army Combat Capabilities Development Command Aviation & Missile Center
Hampton, VA, USA

Leonard V. Lopes
NASA Langley Research Center
Hampton, VA, USA

ABSTRACT

OverFlight is an in-development graphical user interface (GUI) that implements a state-of-the-art rotorcraft maneuvering noise model using a source noise hemisphere approach coupled with the Aircraft NOise Prediction Program 2 (ANOPP2). This GUI stems from a demand for easy-to-use mission planning and community impact acoustic tools that can model the maneuvering flight of a rotary-wing vehicle. This paper covers the models used for the development of OverFlight and model validation efforts. Data from a joint NASA/Army flight test of an MD530F aircraft are used both for source noise hemispheres as well as maneuvering flight data. Analysis of the predicted maneuvering noise shows better agreement that traditional methods currently employed, while also demonstrating maneuvers where the underlying assumptions fail to hold.

NOTATION

a_{lon}	Longitudinal acceleration $[m/s^2]$
A_{jk}	Area of the sub-triangle containing the edge jk
A_T	Area of the triangle containing desired flight condition
g	Gravitational acceleration $[m/s^2]$
$\hat{k}$	Normalized "up" vector
$\hat{n}_a$	Normalized inertial acceleration vector
n_z	Load factor
S_{jk}	Sound pressure level of a one-third octave band [dB]
t	Time [s]
$\hat{u}$	Normalized "Inertial tip-path plane" vector
w_{jk}	Barycentric weights
$\vec{v}$	Inertial velocity vector $[m/s^2]$
V	Freestream velocity $[m/s^2]$
ϕ	Vehicle roll angle [°]
θ	Vehicle pitch angle [°]
γ	Flight path angle [°]
γ_e	Effective flight path angle [°]

INTRODUCTION

Flight operations planning has long been a tool to reduce helicopter noise in and around communities. This often takes the form of designing landing approaches around busy airports and helipads such that noise is abated in sensitive parts of the community (Refs. 1–4). For this purpose, predictions of this sort must be computationally inexpensive to support simulating the number of vehicles in operation around an area of interest. To that end, acoustic hemisphere-based approaches have become the industry standard in rapid acoustic prediction and are implemented in tools such as the Rotorcraft Noise Model (RNM) (Ref. 5), the Advanced Acoustic Model (AAM) (Ref. 6), as well as the European Union Aviation Safety Agency's NORAH (Ref. 7) and NORAH2 (Ref. 8) models.

Traditionally, maneuvering flight has been modeled by dividing a trajectory into straight line segments and using the speed and flight path angle of the vehicle to look up an acoustic hemisphere from a provided database. This approach was extended by Goplan and Schmitz (Refs. 9, 10) with the quasi-static acoustic mapping (Q-SAM) method, which applies a correction to the flight path angle based on the longitudinal acceleration of the vehicle. In 2020, Greenwood and Rau (Ref. 11) published an updated model that extends the Q-SAM approach by modeling the vehicle as a simple point mass that allows for computing an approximate change in roll and pitch angles through a maneuver. The computed change in orientation is then applied to the hemisphere rather than keeping it horizon fixed. Further, they demonstrated that including thrust as an independent lookup variable significantly improved agreement against measurements. However, this model has not made it into any generally available software nor been coupled with more sophisticated acoustic propagation models.

The research presented in this paper takes the model developed by Greenwood and Rau, couples it with NASA Langley's Aircraft NOise Prediction Program 2 (ANOPP2) (Ref. 12) for acoustic propagation, and shows the effectiveness of vehicle load factor corrections when thrust is not an available lookup parameter. Validation and verification is

Presented at the Vertical Flight Society's 82nd Annual Forum & Technology Display, West Palm Beach, FL, USA, May 5–7, 2026.

shown using the dataset gathered by the NASA/Army Comprehensive Rotorcraft Acoustics Flight Test Team (CRAFTT) at the Sierra Army Depot's Amedee Army Airfield (Ref. 13) in 2024.

METHODOLOGY

OverFlight is a new graphical user interface (GUI) in development at NASA's Langley Research Center that is intended to ease the generation of acoustic predictions for rotorcraft operations. While OverFlight supports several modes of operation, this paper focuses on the maneuvering flight model for flight path predictions. OverFlight makes heavy use of ANOPP2 to model acoustic propagation from a source noise hemisphere to observers on the ground. Figure 1 shows a flow chart describing a single timestep of the maneuvering flight model with ANOPP2 components bolded and highlighted in red. Every timestep, OverFlight takes a flight path, built either using the GUI or from a provided file, and computes the kinematics at time t, providing vehicle position, velocity, and accelerations. The kinematics data are passed into the dynamics model, described later, to compute the vehicle's effective flight path angle, roll angle, pitch angle, and load factor. Using the speed and effective flight path angle, a database of hemispheres is queried for the specific flight condition. If no hemisphere is within tolerance then a new hemisphere is interpolated. With the vehicle's state determined and hemisphere selected, the ANOPP2 Straight Ray Propagation Internal Functional Module (ASRPIFM) is used to propagate the source noise to the observers on the ground. Atmosphere, ground, and observer settings all leverage various ANOPP2 data structures to pass the relevant data to ASRPIFM.

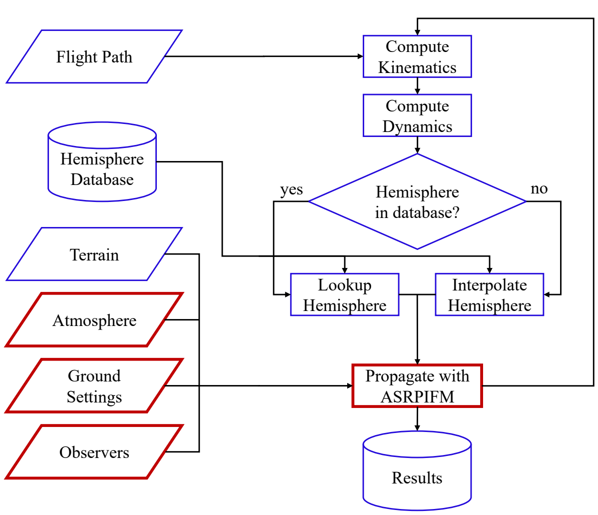

Figure 1: Flow chart describing a single timestep of the maneuvering flight model.

OverFlight is architected with the future in mind, planning for extensions that enable the simulation of different types of vehicles. The intent is to enable easy flight path simulation for both eVTOL and fixed-wing vehicles in the future. The design of the hemisphere database enables easy extension to higher dimensions. This will allow for more independent lookup variables that are required for eVTOL aircraft. The dynamics model is also built in a modular fashion that can be swapped out for different or more sophisticated models, depending on the vehicle and flight condition.

Hemisphere Database

The hemisphere database is a collection of hemispheres that can be generated either from flight test measurements or computational simulations. These hemispheres traditionally have at least 2 independent lookup variables for rotorcraft: flight path angle and speed. The assumption is that these variables fully describe the aerodynamic and thus acoustic state of the vehicle. In reality, thrust has been shown to have significant impact when simulating maneuvering flight (Ref. 11). When stepping through a flight path, the flight path angle and speed are determined at each timestep and the database is queried for an appropriate hemisphere. If a hemisphere already exists within the database at the requested flight condition (within a specified tolerance), then that hemisphere is returned. Otherwise, the database interpolates a new hemisphere based on the provided hemisphere database. To do so, the hemisphere database triangulates the available flight conditions using the speed and flight path angle as coordinate pairs (V and γ). Using this triangulation, the database selects a triangle that contains the requested point, as shown in Figure 2, and uses barycentric interpolation to derive a new hemisphere. This triangle is subdivided and the barycentric weights are computed by dividing the subdivided triangle areas (A_{12}, A_{23}, and A_{13}) by the total area of the parent triangle (A_T) such that

$$w_{jk} = \frac{A_{jk}}{A_T} \tag{1}$$

where j and k are the points that make up the base of the subdivided triangle as seen in Figure 2. Any given one-third octave band sound level, S_i, can then be computed as:

$$S_i = w_{23}S_1 + w_{13}S_2 + w_{12}S_3 \tag{2}$$

where S_1, S_2, and S_3 are the sound pressure levels (SPLs) of a one-third octave band in the bounding hemispheres 1, 2, and 3. The new interpolated hemisphere is inserted back into the database for future use, but excluded from being used for interpolation.

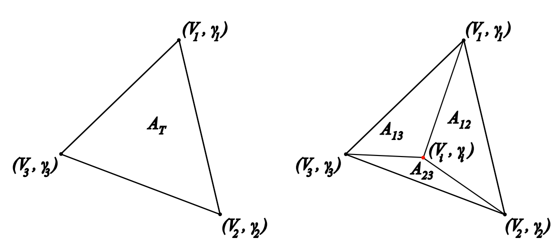

Figure 2: The triangle and subdivided triangle used to interpolate a new hemisphere.

One benefit of this interpolation scheme is that it is easily extensible to higher dimensions by using a higher-order simplex, such as a tetrahedron in three dimensions. This allows usage of a database with more than two independent lookup variables, allowing for the inclusion of thrust.

Maneuvering Noise Model

OverFlight employs a novel model to predict maneuvering noise, first described by Greenwood and Rau (Ref. 11) in 2020. This model generalizes the Q-SAM approach (Refs. 9, 10), wherein the flight path angle is adjusted based on the longitudinal acceleration, a_{lon}:

$$\gamma_e = \gamma + \frac{a_{\text{lon}}}{g}. \tag{3}$$

This approach maps the dynamic flight state to a static flight state by using the effective flight path angle to query the database.

The new model extends this concept by modeling the helicopter as a simple point mass. From this simple dynamics model, the accelerations in all three dimensions can be computed. This allows for the computation of the roll angle, pitch angle, and load factor. The effective flight path angle is now computed as a function of the vehicle's velocity vector $\vec{v}$, the freestream velocity V, and the vehicle's normalized acceleration vector $\hat{n}_a$, shown in equation 4.

$$\sin\gamma_e = \frac{\vec{v}\cdot\hat{n}_a}{V}. \tag{4}$$

A key feature of the model is that instead of keeping the hemisphere horizon fixed, the dynamics model approximates the change in pitch and roll angle of the vehicle, which can then be applied to the hemisphere. This is done by first projecting the vehicle's velocity vector onto the helicopter's tip-path plane, shown in equation 5.

$$\hat{u} = \frac{\vec{v} - (\vec{v}\cdot\hat{n}_a)\hat{n}_a}{V}. \tag{5}$$

For each steady-state hemisphere, the vehicle will be at a certain pitch angle defined by the flight conditions. While this pitch angle does not need to be directly known, a change in pitch angle from the state represented by the hemisphere to the maneuvering state can be computed as

$$\sin\Delta\theta = u_z. \tag{6}$$

Likewise, the change in roll angle is

$$\tan\Delta\phi = \frac{(\hat{k}\times\hat{u})\cdot\hat{n}_a}{\hat{n}_a\cdot(\hat{u}\times\hat{k}\times\hat{u})} \tag{7}$$

where $\hat{k}$ is a normal vector in the "up" direction relative to the inertial frame. The effective flight path angle is then used for the hemisphere database lookup, while the pitch and roll angles are applied to the hemisphere during the simulation (Ref. 11).

Propagation Model

OverFlight leverages ASRPIFM to compute acoustic propagation. As the name states, ASRPIFM implements propagation as a straight ray, ignoring ray curvature effects due to wind or atmospheric variations. Acoustic attenuation is simulated as combination of spherical spreading and atmospheric absorption. The OverFlight user interface allows the user to define an atmosphere profile of varying pressures, temperatures, and humidity as seen in Figure 3. These layers are then used in conjunction with one of the selectable atmospheric absorption models available:

- SAE ARP 866A (Ref. 14)
- 1978 ICAO (Ref. 15)
- ANSI S1.26-1978 (Refs. 16, 17)
- ANSI S1.26-2014 (Ref. 18)

The atmosphere can vary in altitude but otherwise is spatially constant.

ASRPIFM also employs two models for modeling ground reflection and absorption. Ground reflections are modeled based on theory developed by Chien and Soroka (Ref. 19) while the ground impedance model is based on theory developed by Attenborough (Ref. 20). Since the Chien and Soroka theory is developed for a point source, ASRPIFM extends the model to allow for both a single emission angle or dual emission angle approaches when the point source assumption is not valid.

RESULTS

To validate and verify the OverFlight noise model, an experimentally produced database of an MD530F is used. Properties of interest for the MD530F can be found in Table 1 (Ref. 13). The dataset was gathered by CRAFTT at the Sierra Army Depot's Amedee Army Airfield (Ref. 13) in 2024. This flight test captured several steady flight conditions that were used to create a database of 123 hemispheres for use in tools such as AAM and OverFlight. These hemispheres were created using a snapshot-style microphone array rather than a traditional linear array. This same test campaign also captured several maneuvers (Ref. 21), some of which are used for this validation and verification. The specifics of each run can be seen in Table 2.

Table 1: Vehicle Characteristics.

No. Main Rotor Blades	5
Main Rotor RPM/BPF	477 / 39.75 Hz
No. Tail Rotor Blades	2
Tail Rotor RPM/BPF	2848 / 94.9 Hz

Overall and A-Weighted sound pressure level (OASPL and OASPLdBA) and select one-third octave band SPLs are examined in the following sub-sections. Of particular interest

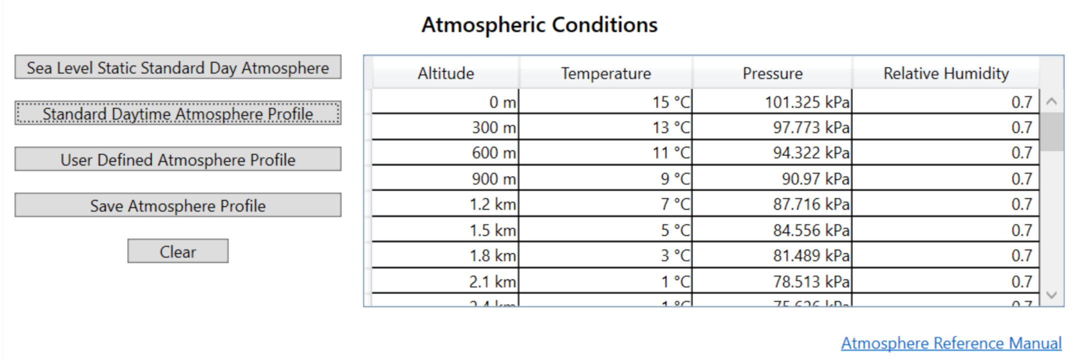

Figure 3: GUI for setting up atmospheric layers.

Table 2: Maneuver Flight Conditions.

Condition Code	Description	Maximum Roll Rate	Maximum Pitch Rate
M1	Fast cyclic roll right	$55.4\,^\circ/s$	$17.4\,^\circ/s$
M3	Slow cyclic roll right	$13.3\,^\circ/s$	$3.0\,^\circ/s$
M6	Collective pitch up	$10.5\,^\circ/s$	$11.9\,^\circ/s$

are the 40 Hz band frequency, which is centered close to the blade-passing frequency (BPF) of the main rotor, the 100 Hz band frequency, which is centered close to the BPF of the tail rotor, and the 200 Hz band frequency that is centered close to the second tail rotor BPF and the fifth main rotor BPF. Due to the sensitive nature of the vehicle, all results are displayed using a relative SPL value rather than an absolute value. The maximum measured SPL per microphone per run per octave is used as a reference value for all following SPL figures. All times are relative to when the vehicle passes over the center of the array. The measured data are processed by segmenting the acoustic pressure time histories into 0.5-second chunks with 0.25 seconds of overlap. Each chunk is then converted into both a narrowband spectrum to integrate the OASPL and OASPLdBA and a one-third octave SPL spectrum to examine specific frequency bands.

For this validation and verification, OverFlight imports a file that includes a series of positions of the vehicle about a geodetic datum point and the velocities of the vehicle at each point. These files were created directly from the flight test data, where the positions and velocities were pre-processed with a smoothing spline to ensure clean derivatives in OverFlight. OverFlight then takes these points and uses an Akima cubic spline (Ref. 22) to interpolate the path to arbitrary points in time. The vehicle acceleration and heading are computed along the path using the provided velocities, which in turn are provided to the dynamics model to compute the remaining values at each timestep. Since the database is derived from experimental data, it only includes speed and flight path angle as independent lookup variables and neglects thrust. To compensate, a correction of $20.0\log_{10}(n_z)$, where n_z is the load factor computed by the dynamics model, is applied across the spectrum (Ref. 11).

Steady Fly-Over

Before maneuvers, a simple 90-knot steady fly-over is presented. While this case is trivial, it demonstrates the setup and format of the following maneuver discussions. It also serves a simple check case as a first step in verification of coupling between the different components. Figure 4 shows the microphone layout and the trajectory of the vehicle over the array. The two starred microphones are analyzed through both integrated metrics as well as the specific one-third octave bands discussed above.

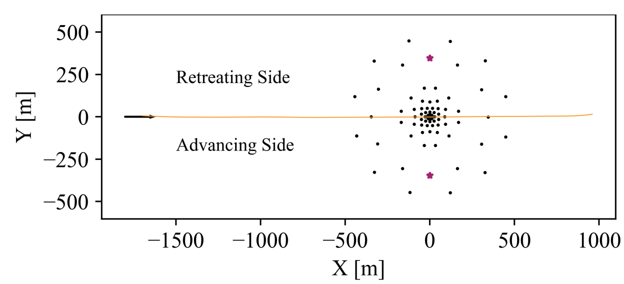

Figure 4: Microphones used to examine the steady level fly-over.

On the retreating side, Figure 5 shows integrated SPL time histories as the vehicle flies over the array for four different cases: 1) the measured noise, 2) the full OverFlight maneuvering noise model, 3) the maneuvering noise model, neglecting load factor correction, 4) the traditional Q-SAM approach, neglecting hemisphere orientation correction. Both OASPL and OASPLdBA are underpredicted by OverFlight by 6 dB in some instances. The one-third octave bands in Figure 6 show that the lower bands follow closely with measurement when the vehicle is crossing over the array, between -10 and 10 seconds. The 40 Hz and 100 Hz frequency bands also predict the dip in SPL at array crossover, with it being overpredicted in the 40 Hz frequency band. However, the 200 Hz frequency band shows OverFlight underpredicting the values for most of the flyover. There is also significant error in the 40 Hz frequency band leading up to the array that isn't seen in the other frequency bands. This discrepency in the lower frequency is likely due to background noise due to the wind. This background noise can be heard early in the recording and is more pronounced than the vehicle itself at far distances. The background noise is absent from the OverFlight prediction, thus causing it to show lower levels in the 40 Hz frequency band.

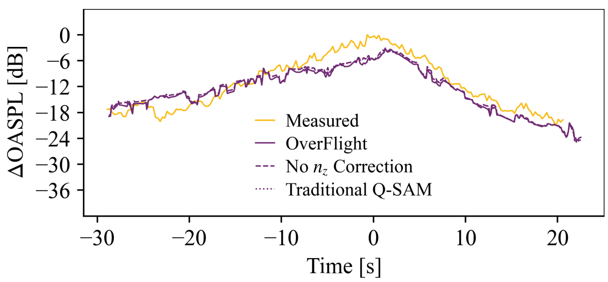

(a) OASPL

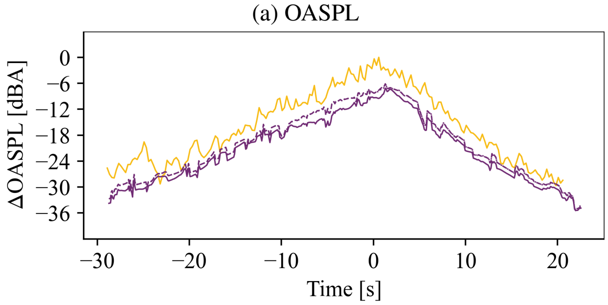

(b) OASPLdBA

Figure 5: Retreating side integrated sound level for the steady level fly-over.

However, the advancing side shows better integrated trends than the retreating side, as seen in Figure 7. OASPLdBA shows slightly worse agreement than OASPL, underpredicting between -10 and 10 seconds. The one-third octave bands shown in Figure 8 also show good agreement, with the 200 Hz frequency band underpredicting both near the peak and after the 10-second mark. The 40 Hz frequency band shows the same discrepancy leading up to the array seen on the retreating side as well, likely due to the recording containing background noise.

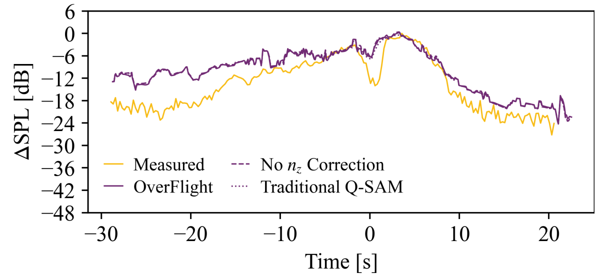

(a) 40 Hz

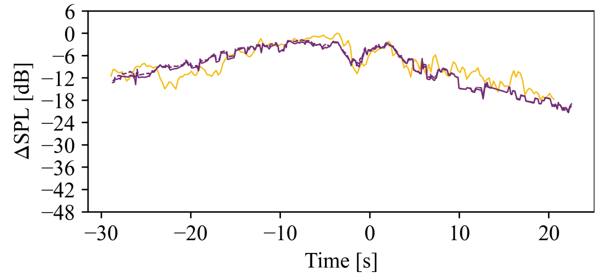

(b) 100 Hz

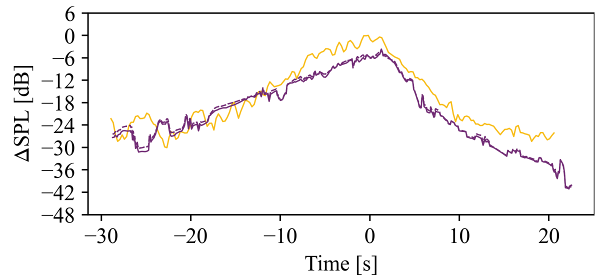

(c) 200 Hz

Figure 6: Retreating side one-third octave bands for the steady level fly-over.

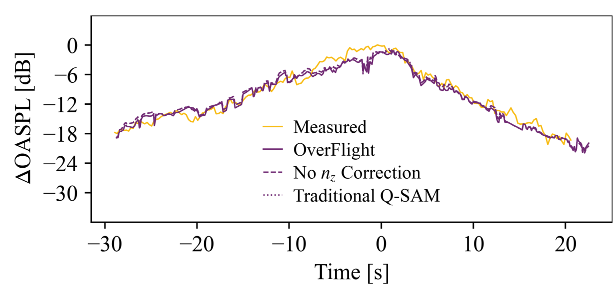

(a) OASPL

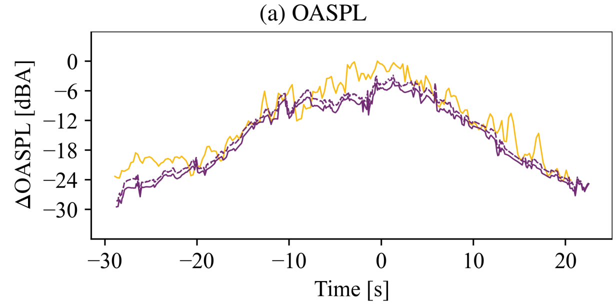

(b) OASPLdBA

Figure 7: Advancing side integrated sound level for the steady level fly-over.

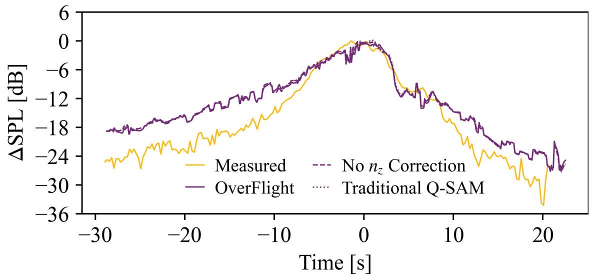

(a) 40 Hz

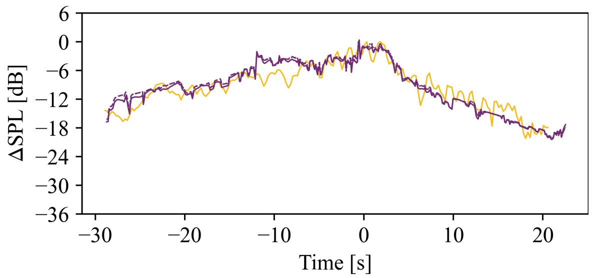

(b) 100 Hz

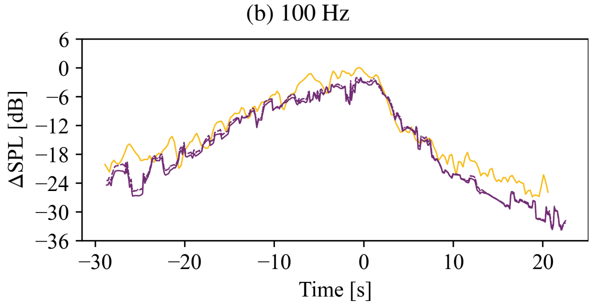

(c) 200 Hz

Figure 8: Advancing side one-third octave bands for the steady level fly-over.

Perhaps counterintuitively, the advancing side exhibits lower peak OASPL and OASPLdBA values than the retreating side by 2 dB and 6.5 dBA in the measurement. This seems to stem from the higher harmonics of the tail rotor, as the lower frequency bands show higher levels on the advancing side as one might expect due to convective amplification. As a steady level flight condition should put the main rotor into a state where lower harmonics dominate, it's likely the rise in levels in the higher frequency bands emanates from the tail rotor. Since the tail rotor is situated on the left side of the vehicle, the advancing side has some shielding from the tail rotor due to the vertical stabilizer, thus showing lower integrated peak levels. Since the lower frequency bands show close agreement of peak values, it's possible that the tail rotor's aerodynamic state during the experiment was influenced by the wind, aggravating tail rotor blade-vortex interaction (BVI). As the prediction operates from the main rotor state, a difference in tail rotor aerodynamic state is not accounted for. This discrepancy between prediction and measurement is reduced when looking at a retreating side microphone closer to the center of the array as seen in Figure 9. This microphone is closer to in-plane with the tail rotor, while being more out-of-plane of the main rotor, thus lowering the tail rotor's loading noise contribution and increasing the main rotor's loading noise contribution. This further supports that the discrepancies seen on the retreating side microphone stem from tail rotor noise.

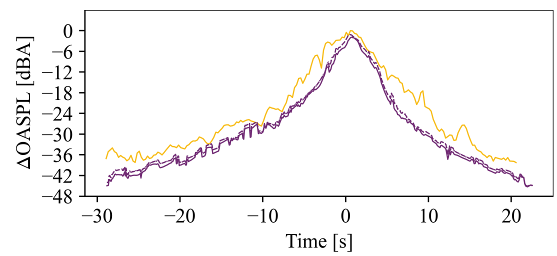

Figure 9: OASPLdBA of a retreating side microphone closer to the center of the array.

Slow Cyclic Roll Maneuver

The first maneuver is a "slow" cyclic roll, designated M3, where the vehicle initiates the roll just before the center array microphone, achieving a maximum roll angle of 43.5°. Figure 10 shows the trajectory of the vehicle over the array with two microphones highlighted, one on the advancing side and one on the retreating side. These microphones are selected to show the impact of the orientation correction applied to the hemisphere, as they see a large change in source emission angle due to the rolling motion of the vehicle while keeping the emission angles inside the available source noise data. Microphones further out on the advancing side have source emission angles above the tip-path plane of the vehicle where there are no acoustic data, thus providing incorrect results.

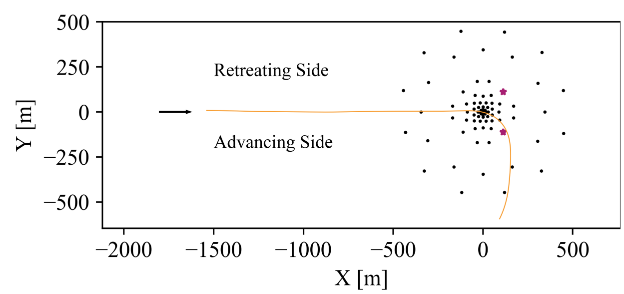

Figure 10: Microphones used to examine the slow cyclic roll maneuver.

The roll angle predicted by OverFlight, shown in Figure 11, follows closely with the measured roll angle on the vehicle underpredicting the maximum roll angle by 2.2°. Figure 12a shows the OASPL for both the advancing and retreating side microphones as a function of time. The retreating side microphone underpredicts OASPL levels but matches the trend well, as OverFlight captures the dip in levels at the crossover point where the traditional Q-SAM approach does not. A similar trend is observed when looking at the OASPLdBA values for the same microphone, as seen in Figure 12b. The full model not only captures the dip in levels, it also predicts the first hump to have a slightly lower amplitude than the second. The load factor through this maneuver remains relatively low, thus most of the improvement in results over the traditional Q-SAM approach is due to the orientation correction of the hemisphere. While the overall levels are underpredicted, the general trend is improved over the traditional Q-SAM approach.

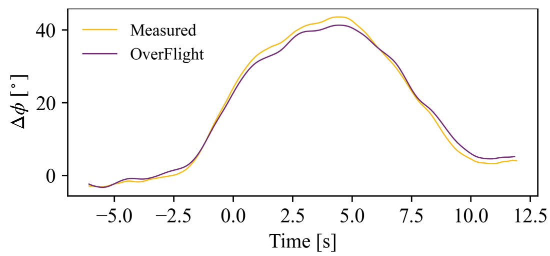

Figure 11: Roll angle vs time for the slow cyclic roll maneuver.

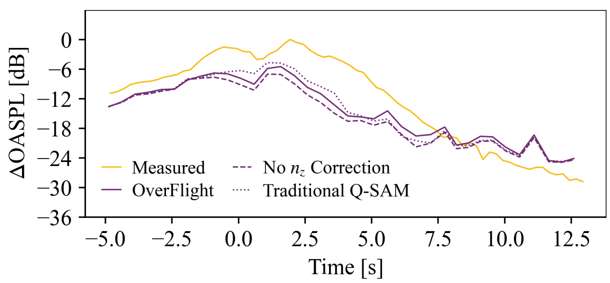

(a) OASPL

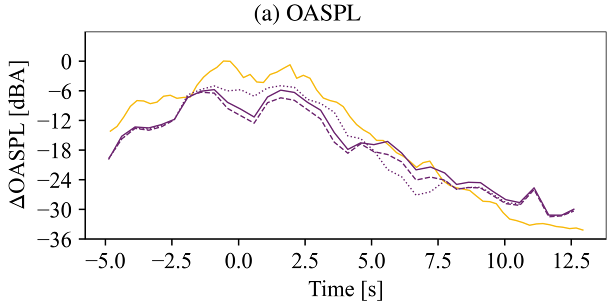

(b) OASPLdBA

Figure 12: Retreating side integrated sound level for the slow cyclic roll maneuver.

The one-third octave bands shown in Figure 13 show the 40 Hz frequency band follows levels well until the 1-second mark when prediction diverges from measurement. A similar trend is seen in the 100 Hz frequency band as well. However, the 200 Hz frequency band shows better agreement across the maneuver. The first peak at the crossover point is significantly underpredicted, while the levels of the second peak are closer, but are lead by the prediction by about one second. The retreating side underprediction is consistent with the steady level fly-over, however likely for a different reason. For this maneuver, the retreating side microphone shows a peak value that is 9 dB (7 dBA) lower than the advancing side microphone. This means that, proportionally, more of the integrated acoustic energy on the retreating side is from sources other than the vehicle, inflating the integrated metrics seen in the measurement. On the advancing side the vehicle dominates over other sources, so the integrated metrics should contain more vehicle noise. As OverFlight does not include background noise in its predictions, it predicts a lower value than seen in measurement.

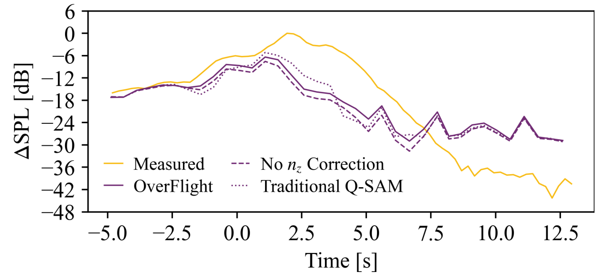

(a) 40 Hz

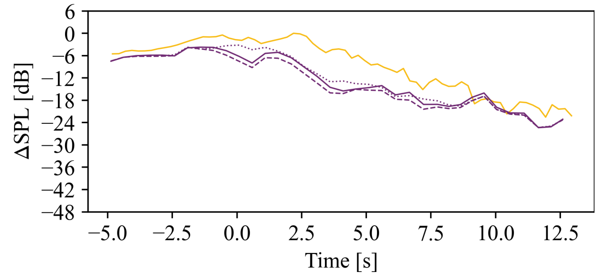

(b) 100 Hz

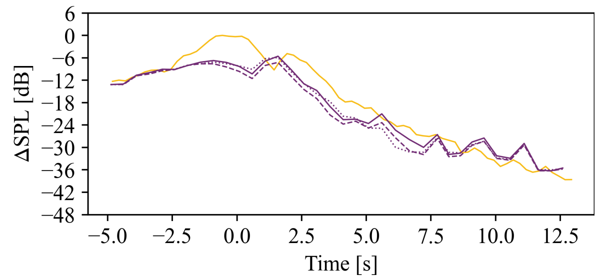

(c) 200 Hz

Figure 13: Retreating side one-third octave bands for the slow cyclic roll maneuver.

Figure 14 shows the integrated levels at the advancing side microphone. OverFlight tracks the measured OASPL well across the maneuver, matching levels and directivity. The full model corrects a slight directivity error seen in the traditional Q-SAM approach, matching the time of the peak values and the subsequent falloff better. The OASPLdBA shows slightly worse agreement, predicting the peak well but falling off faster than measurement and the traditional Q-SAM approach. The one-third octave bands shown in Figure 15 show reasonable agreement of peak levels. However, there exists significant error in the levels approaching the peak with OverFlight overpredicting in both the 40 Hz and 100 Hz frequency bands, missing the dip that happens in both bands. Falloff in the 40 Hz frequency band shows good agreement until the 7.5-second mark where it diverges from measurement. The 200 Hz frequency band shows better agreement across the maneuver.

Overall, the addition of attitude correction improves the result of the simulation, fixing directivity errors that arise when the orientation of the hemisphere is ignored. While significant underprediction exists on the retreating side, OverFlight pre-

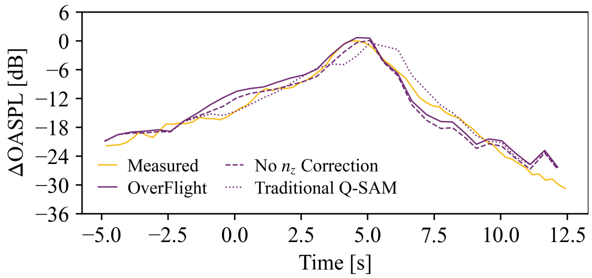

(a) OASPL

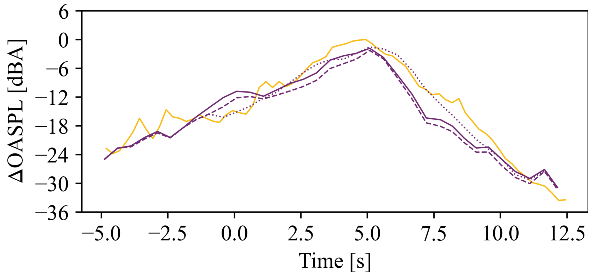

(b) OASPLdBA

Figure 14: Advancing side integrated sound level for the slow cyclic roll maneuver.

dicts the trends better than the traditional Q-SAM approach. Retreating side discrepancies are suspected to, at least partially, stem from additional acoustic energy, either from electrical measurement noise or background noise. Additionally, there is slight improvement to the predictions by artificially applying a variation to the effective flight path angle in the simulation. This implies that either some of the error stems from the simple point mass model, or the flight path angle associated with the measured hemispheres contains some error.

Fast Cyclic Roll Maneuver

Following the "slow" cyclic roll maneuver, a much more aggressive roll maneuver, designated M1, will now be examined. Similar to the previous maneuver, two microphones are examined, one on the advancing side and one on the retreating side as highlighted in Figure 16. Figure 17 shows the roll angle with respect to time. This maneuver reached a maximum roll angle of 71.6° with a maximum roll rate of $55.4°/s$ with OverFlight only underpredicting the maximum roll angle by half a degree. This tracks the measured roll angle through the maneuver well. During the maneuver the helicopter experienced a maximum load factor of 1.9, making this a rather aggressive maneuver. This maneuver initiates just before the vehicle passes over the center of the array and last for roughly 10 seconds. Therefore the acoustic results focus in that same time region, adjusted for propagation time.

Much like the previous cases, the retreating side integrated levels, shown in Figure 18, underpredict the levels through the maneuver. The peak values are generally well predicted in time, but OverFlight underpredicts the levels by 12 dB. Nonetheless, the maneuvering flight model still performs better than the traditional Q-SAM approach. It's also clear the load factor correction plays a large role in this maneuver,

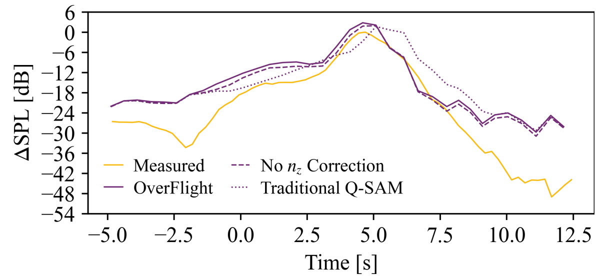

(a) 40 Hz

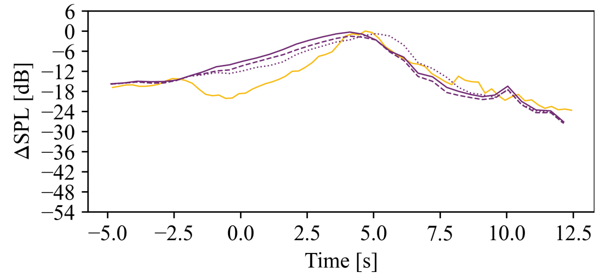

(b) 100 Hz

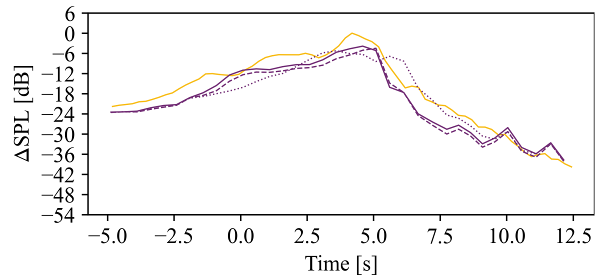

(c) 200 Hz

Figure 15: Advancing side one-third octave bands for the slow cyclic roll maneuver.

applying a 6 dB increase in levels over the uncorrected prediction. The one-third octave bands in Figure 19 shed some light on where the underprediction stems from. The 40 Hz frequency band shows the largest amount of underprediction through the maneuver while missing the double "hump" seen in the measurement. The 100 Hz frequency band performs well, showing better agreement than the traditional Q-SAM model. The 200 Hz frequency band also underpredicts levels from the crossover point till the end. This band shows slightly better trends than the 40 Hz band, showing a slight double "hump" where the measurement shows a more significant second peak.

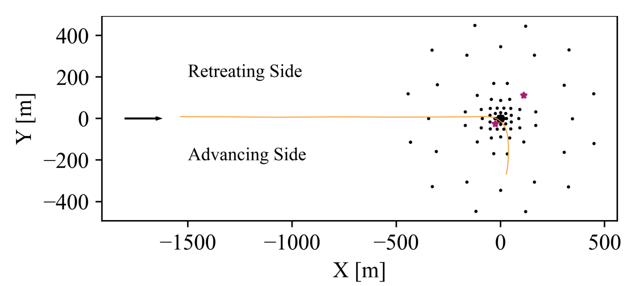

Figure 16: Microphones used to examine the fast cyclic roll maneuver.

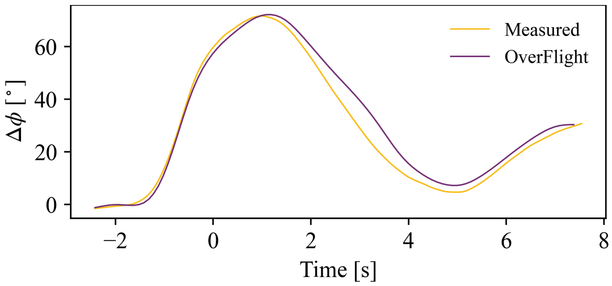

Figure 17: Roll angle vs time for the fast cyclic roll maneuver.

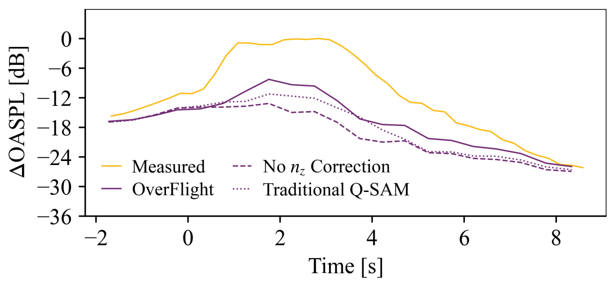

(a) OASPL

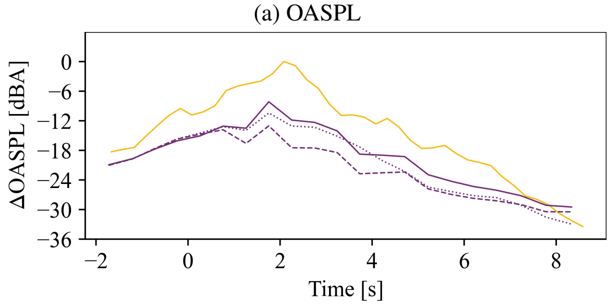

(b) OASPLdBA

Figure 18: Retreating side integrated sound levels for the fast cyclic roll maneuver.

The advancing side OASPL and OASPLdBA are seen in Figure 20. The measured OASPL has three slight peaks, while the prediction shows a singular large peak followed by rapid decay. A similar trend is seen in the OASPLdBA levels where OverFlight predicts a singular large peak that overpredicts levels. The one-third octave bands, shown in Figure 21, show OverFlight overpredicting the 40 Hz frequency band with the peak value arriving late. However, while the traditional Q-SAM model predicts the peak levels better, the maneuvering model predicts the peak time better. The 100 Hz frequency band shows OverFlight only slightly overpredicting the levels while arriving earlier than in measurement. Finally, in the 200 Hz frequency band, OverFlight predicts both the peak levels and time correctly, but shows significant error in the falloff. There are a number of potential issues with this maneuver, both with the model and the dataset used. As stated previously, the maximum roll angle experienced by the vehicle through this maneuver was over 70°, which puts the emission angle near the horizon of the hemisphere for this microphone. Further, the simple point mass dynamics model has trouble keeping up with the rapid changes in pitch angle as seen in Figure 22. The vehicle undergoes a pitch rate in excess of $17^\circ/s$ where the dynamics model cannot keep up. This means

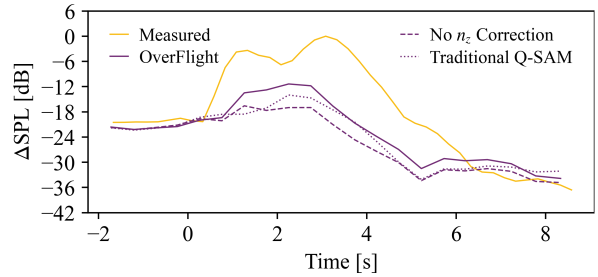

(a) 40 Hz

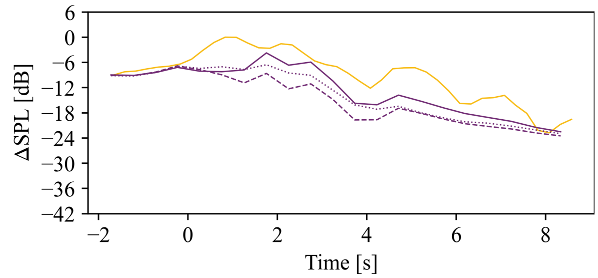

(b) 100 Hz

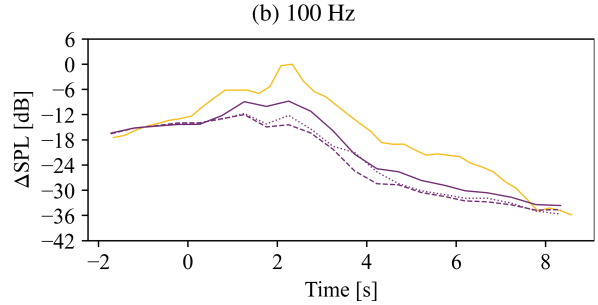

(c) 200 Hz

Figure 19: Retreating side one-third octave bands for the fast cyclic roll maneuver.

that through the maneuver, the pitch orientation of the hemisphere differs significantly from the actual vehicle.

This maneuver shows some of the limits of this maneuvering noise model. The systemic issue of underprediction on the retreating side still exists, and the advancing side prediction suffers from near-horizon emission angles. Further, the misprediction of pitch rate and thus pitch affects all microphones. This raises the possibility of using a more sophisticated dynamics model that models the distributed mass of an actual helicopter with associated rotor dynamics. While such a model could capture transients better than the point mass model, more vehicle-specific characteristics would need to be provided, negating the simplicity of the current method. Further, maneuvers with high roll rates can cause vortex bundling on the advancing side of the rotor that can amplify BVI noise. Since this vortex bundling is a result of the high roll rate, the Q-SAM assumption fundamentally cannot capture this aeroacoustic phenomenon. Stutz et al. (Ref. 21) demonstrated high levels of BVI in the region where both microphones are, supporting this hypothesis. The use of maneuvering noise hemispheres could aid in improving results for maneuvers that undergo large roll rates, making roll rate another database lookup parameter. A method of creating such hemispheres has been developed by the German Aerospace Center (DLR), but

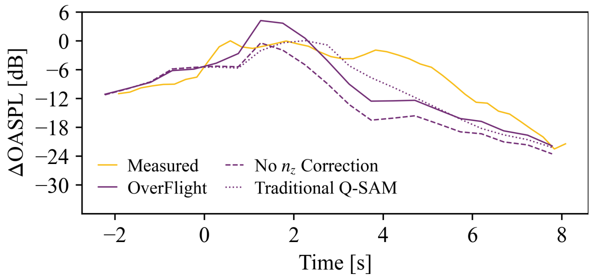

(a) OASPL

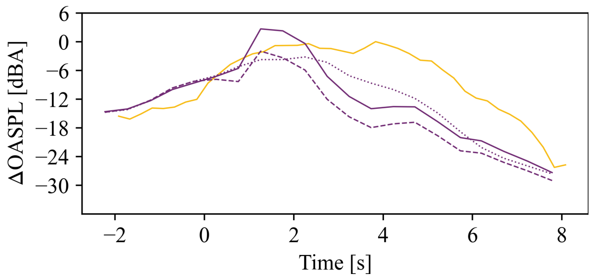

(b) OASPLdBA

Figure 20: Advancing side integrated sound level for the fast cyclic roll maneuver.

has not seen wide application due to the challenges of creating a database that covers all feasible maneuvers (Refs. 23, 24).

Collective Pitch Up Maneuver

The final maneuver is a collective pitch up maneuver. While this maneuver doesn't exhibit a particularly large roll or pitch rate, it does extend outside the available data in the database. This is true of all the pitch up maneuvers recorded as part of the flight test. Specifically, the effective flight path angle shown in Figure 23 reaches roughly 30° whereas the database only includes positive flight path angles up to 6.4°. Nonetheless, several of the results, especially integrated metrics, appear reasonable through the maneuver. Two microphones, one advancing side, the other retreating side, are selected to analyze the results from the maneuver and are shown in Figure 24.

Figure 25 shows the integrated metrics through the maneuver on the retreating side. The OASPL tracks well through the maneuver, capturing the dip in levels around the 5-second mark. The OASPLdBA, seen in Figure 25b, tracks well to start but diverges around the 5-second mark implying an error in certain frequency bands. This is where the vehicle finishes the pitch-up and rolls to turn away from the microphone array, putting the vehicle into a more dynamic state. Figure 26 shows that OverFlight overpredicts levels in the 40 Hz frequency band between -4 seconds and 4 seconds where the measurement shows the levels dip down. However, looking at the 100 Hz frequency band SPL shows better agreement along the maneuver showing that the tail rotor state is not far off. The 200 Hz frequency band is where the divergence seen in the OASPLdBA stems from. While the integrated values on the hemisphere may be close to what was measured, the specific frequency components do not necessarily match due

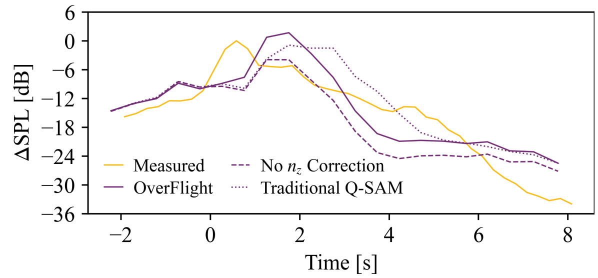

(a) 40 Hz

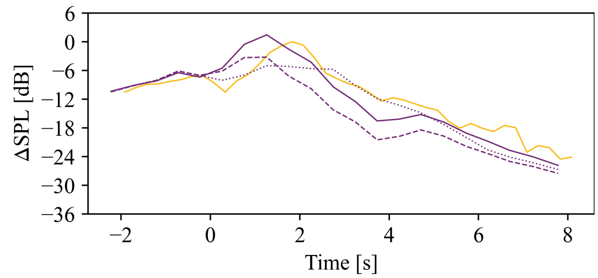

(b) 100 Hz

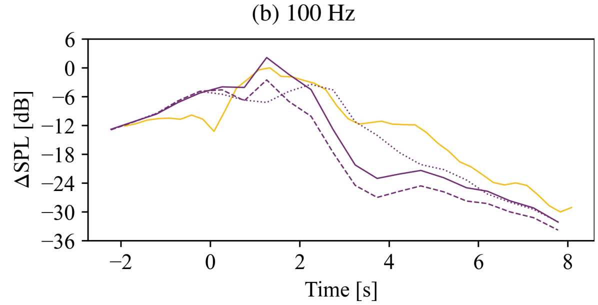

(c) 200 Hz

Figure 21: Advancing side one-third octave bands for the fast cyclic roll maneuver.

to the mismatch in the rotor's aerodynamic state due to the large predicted effective flight path angle. Further, at the end of this maneuver, the dynamics model is not capturing enough of the vehicle dynamics to compute the correct change in pitch angle. This can be seen in Figure 27, which shows the pitch rate predicted by OverFlight compared against the measured pitch rate. OverFlight predicts the pitch rate with reasonable accuracy through the bulk of the maneuver between the crossover point to the 5-second mark. Past the 5-second mark, where the acoustic agreement suffers, the simple point mass model does not predict the rapidly changing pitch rate seen in measurement. Thus, the pitch computed by OverFlight does not match reality and thus prediction accuracy suffers. Ad-

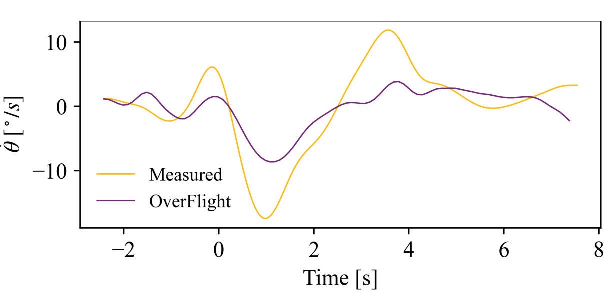

Figure 22: Pitch rate vs time for the fast cyclic roll maneuver.

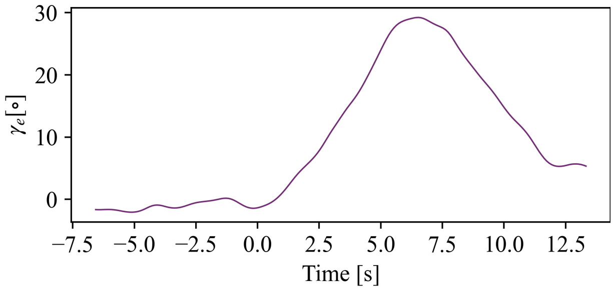

Figure 23: Predicted effective flight path angle through the collective pitch up maneuver.

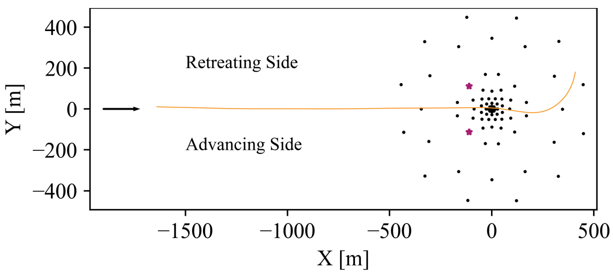

Figure 24: Microphones used to examine the collective pitch up maneuver.

ditionally, OverFlight's roll angle prediction, seen in Figure 28, loses accuracy past the 10-second mark, predicting much more variation in the roll angle than seen in measurement.

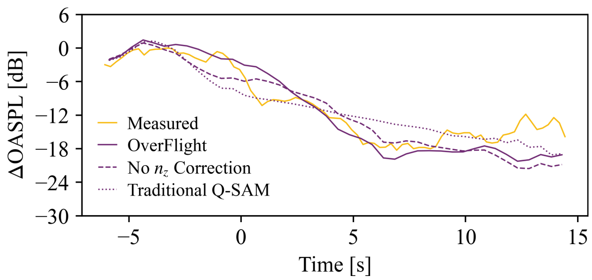

(a) OASPL

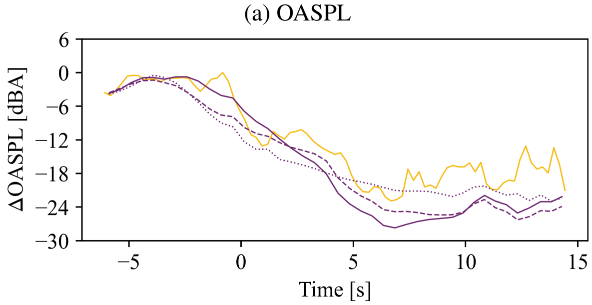

(b) OASPLdBA

Figure 25: Retreating side integrated sound levels for the collective pitch up maneuver.

On the advancing side, the integrated levels match better through the initial part of the maneuver, with OASPL initially underpredicted, but following the fall off trend closely as seen in Figure 29a. The OverFlight model also captures the trend reversal around the 6-second mark. However, as the vehicle continues into the steepest bank angle, the model underpredicts the levels, likely for similar reasons as discussed for the retreating side. The one-third octave band trends seen in Figure 30 show similar accuracy as the retreating side where the lower bands that contain the main rotor primary BPF and the tail rotor primary BPF track with reasonable accuracy, but the 200 Hz band SPL shows divergence around the 8-second mark. Since both advancing and retreating sides show similar trends as the vehicle banks into a turn, the likely source of error stems from the high effective flight path angle extending outside the bounds of the dataset.

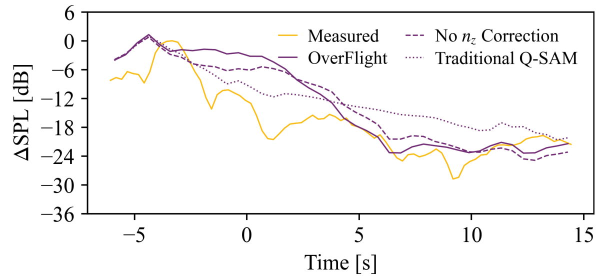

(a) 40 Hz

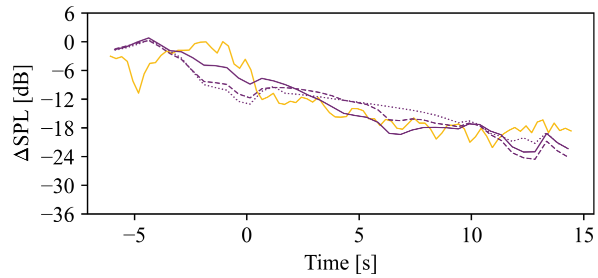

(b) 100 Hz

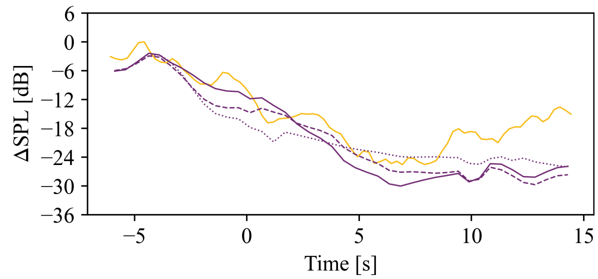

(c) 200 Hz

Figure 26: Retreating side one-third octave bands for the collective pitch up maneuver.

This maneuver pushes the boundary of the maneuvering noise model beyond what's been shown in previous litera-

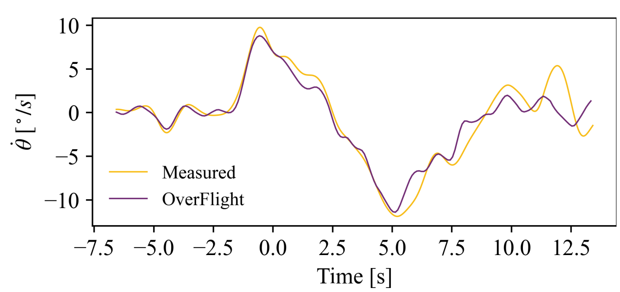

Figure 27: Predicted pitch rate through the collective pitch up maneuver.

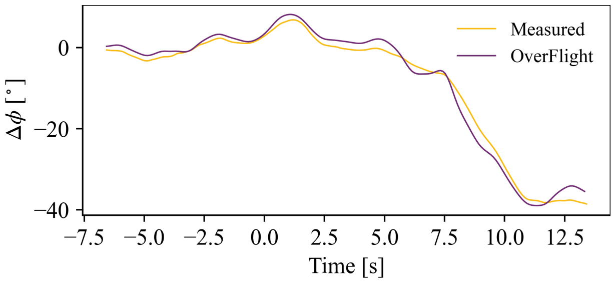

Figure 28: Predicted roll angle through the collective pitch up maneuver.

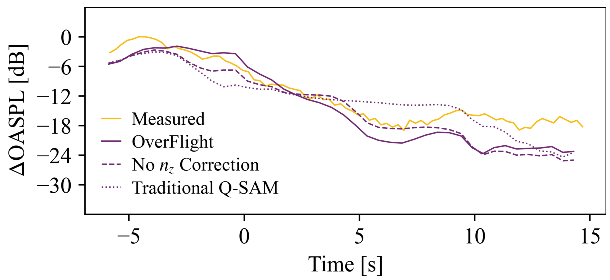

(a) OASPL

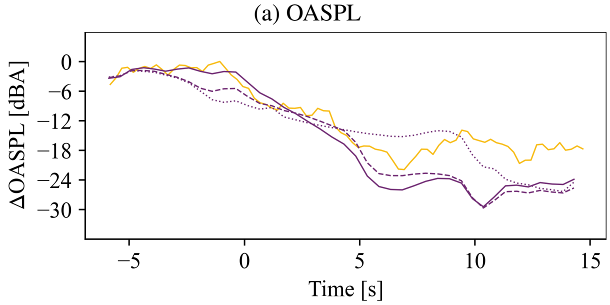

(b) OASPLdBA

Figure 29: Advancing side integrated sound levels for the collective pitch up maneuver.

ture (Ref. 11) while demonstrating better results than a traditional Q-SAM approach that neglects the hemisphere orientation corrections. The errors that exist, specifically past the 10-second mark suggest a possible breakdown of the point mass dynamics assumption, but they are also exacerbated by having insufficient data in the database for the flight conditions. Therefore, if a hemisphere database could be produced using a tuned computational model, one could create a database that includes the extreme flight path angles experienced in this ma-

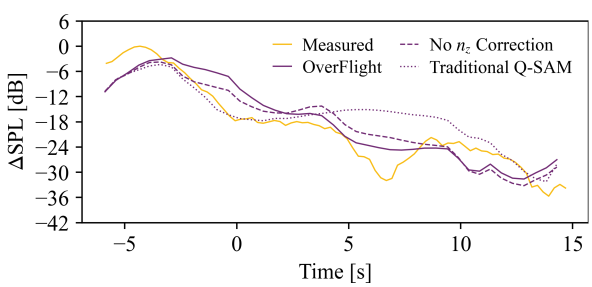

(a) 40 Hz

Figure 30: Advancing side one-third octave bands for the collective pitch up maneuver.

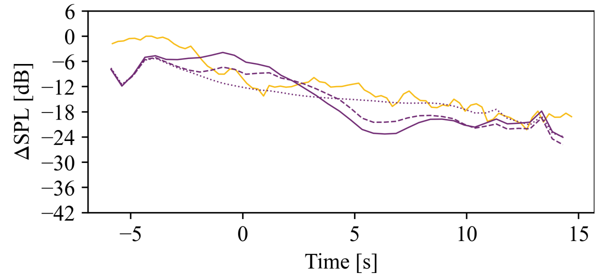

(b) 100 Hz

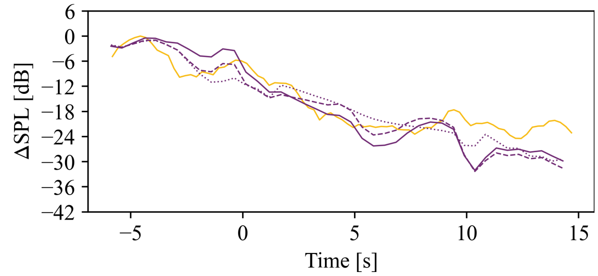

(c) 200 Hz

Figure 30: Advancing side one-third octave bands for the collective pitch up maneuver.

neuver.

GUI CAPABILITIES

OverFlight boasts many features to ease the setup of simulations, examine results, and share the inputs and outputs with colleagues. Workspaces are the top level of organization in OverFlight. Every workspace can have one or more hemisphere databases associated with it, an atmosphere profile, propagation settings, ground observer setup, terrain, and a flight path. Workspaces can be saves to disk to either save session state or to share with other people. The interface also supports copy-paste functionality for all graphical outputs to ease sharing of results. OverFlight also supports the use of Digital Terrain Elevation Data (DTED) in simulations, enabling OverFlight to give better predictions in areas with significant terrain variations. Further, the terrain data are used to compute line-of-sight between the vehicle and ground observers to approximate acoustic shadowing. OverFlight supports several modes of operation: 1) noise-power-distance (NPD) curve mode, meant for certification, 2) single-waypoint mode, which allows for predicting acoustic contours at a single speed and altitude, and 3) flight path mode.

Figure 31 demonstrates the flight path visualization when performing a simulation. The arrows represent the waypoints that define the start and end of a segment. Each waypoint defines the position, speed, and heading of the vehicle. The properties are then interpolated through the segment. Figure 31 also shows the hemisphere used for the selected timestep, oriented as predicted by the dynamic model. The green patches in the result contours are locations where the line-of-sight from the vehicle is obscured. OverFlight allows the user to "scrub" through the timesteps of the simulation, viewing acoustic contours of various metrics on the ground. Acoustic results can be viewed either from an emission timebase or from a common reception timebase. Flight path results can also be exported to produce publication-quality figures. Similar visualization facilities exist for single-waypoint mode as well, allowing the user to explore the impact from the noise of the vehicle on the terrain in 3D. NPD mode generates plots useful in the case of certification activities, replacing the 3D views.

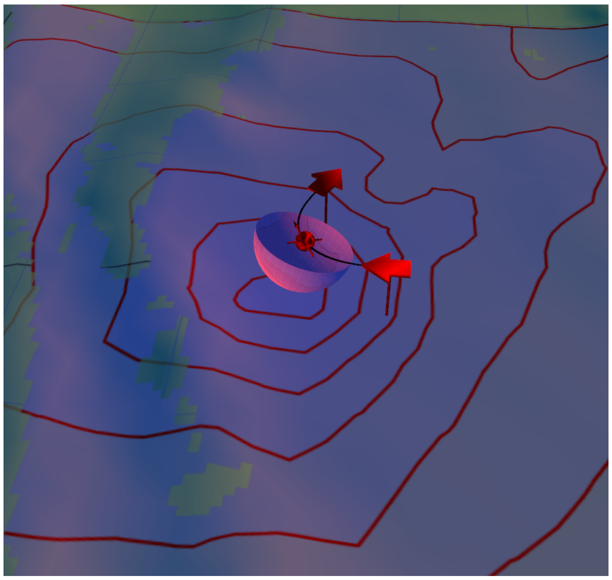

Figure 31: 3D flight path result visualization showing the hemisphere used at that timestep and OASPL contours on the ground.

CONCLUSIONS

In this paper the coupling of a novel maneuvering noise flight model, previously developed by Greenwood and Rau (Ref. 11), with the state-of-the-art propagation models provided by ANOPP2 was developed. Validation and verification was done using several maneuvers that were measured during the Army/NASA joint flight test of an MD530F at the Sierra Army Depot's Amedee Army Airfield. One steady flyover and three maneuvers were selected to compare against with three different comparisons made: 1) the maneuvering noise model with load factor correction, 2) the model without load factor correction, 3) traditional Q-SAM approach that neglects hemisphere orientation corrections. In general, the new model improves prediction accuracy over the traditional Q-SAM approach that only considers longitudinal acceleration and neglects correcting the orientation of the hemisphere. The load factor correction aids in accuracy of maneuvers, especially when considering the integrated acoustic levels, but isn't necessarily applicable across the entire spectrum as applied in this work. This is occasionally seen in the 100 Hz one-third octave band, which contains the tail rotor primary harmonic. This is due to the fact the the load factor primarily impacts the main rotor aerodynamic state, making the correction to certain bands erroneous. To rectify this, a database that is produced computationally should include the main rotor thrust coefficient as an independent lookup variable.

The fast cyclic turn maneuver pushed the boundaries of the simple point mass dynamics model to the point where the predicted pitch rate could not come close to matching measurement. Further, the extreme bank angle puts the emission angles near the horizon for the advancing side microphone that was examined. Microphones that are further out from that point would have emission angles from above the tip-path plane of the vehicle where there are no measured data. This could be potentially resolved with a database produced by computational simulations that can create full spheres of acoustic source noise data. There is also evidence of maneuver-induced BVI that would not be captured through a quasi-static acoustic mapping approach. The collective pitch up maneuver also pushed the boundaries of both the modeling and available data in the hemisphere database, as large positive flight path angles are difficult to measure due to safe starting altitudes leading to larger propagation distances at steep flight path angles. This is yet another area where a computational database could provide better results. Finally, while this maneuver isn't particularly aggressive, the combined pitching and rolling motion of the vehicle puts it into a dynamic state where it appears the point mass assumption may not be valid. A more complete description of the vehicle would be needed that models the distributed mass and rotor dynamics.

Author contact: Robert Rau robert.f.rau@nasa.gov

James Stephenson James.H.Stephenson23.civ@army.mil

ACKNOWLEDGMENTS

The authors would like to acknowledge the ANOPP2 team's Dr. Venkat Iyer and his extensive knowledge when integrating ANOPP2 into OverFlight and the inner workings of ASRPIFM. The authors would also like to acknowledge the NASA/Army Comprehensive Rotorcraft Acoustics Flight Test Team whose data were invaluable to the validation carried out in this paper. Particular thanks go to Mary Houston for her work in assembling the source noise hemisphere database and Dr. Colin Stutz for discussions on the maneuvers that were carried out. Thanks to Dr. Eric Greenwood for his mentorship through the initial development of this model starting back in 2013 with an undergraduate intern.

REFERENCES

1. Watts, M. E., Greenwood, E., Smith, C., and Stephenson, J., "Noise Abatement Flight Test Data Report," NASA TM 2019-220264, NASA Langley Research Center, Hampton, VA 23681, USA, March 2019.

2. Helicopter Association International, *Fly Neighborly Helicopter Noise Abatement Recommendations*, Available at: `https://verticalavi.org/wp-content/uploads/2025/01/zz.FN-Tips-Flyer2_15Nov2019_with-FAA-VAI-Logo.pdf`, Accessed on 15-03-2026.

3. Pascioni, K. A., Greenwood, E., Watts, M. E., Smith, C. D., and Stephenson, J. H., "Medium-Sized Helicopter Noise Abatement Flight Test," Proceedings of the 76^{th} Annual Forum of the Vertical Flight Society, Virginia Beach, VA, October 2020.

4. Stephenson, J. H., Watts, M. E., Greenwood, E., and Pascioni, K. A., "Development and Validation of Generic Maneuvering Flight Noise Abatement Guidance for Helicopters," *Journal of the American Helicopter Society*, Vol. 67, (1), January 2022, pp. 1–12. DOI: 10.4050/JAHS.67.012012.

5. Conner, D., and Page, J., "A Tool for Low Noise Procedures Design and Community Noise Impact Assessment: The Rotorcraft Noise Model (RNM)," Proceedings of Heli Japan, Tochigi, Japan, November 2002.

6. Page, J. A., Wilmer, C., Schultz, T., Plotkin, K. J., and Czech, J., "Advanced Acoustic Model Technical Reference and User Manual," Technical Report WP-1304, SERDP, 2009.

7. Tuinstra, M., and van Oosten, N., "The Development Of A European Helicopter Noise Model," 44th European Rotorcraft Forum, Delft, the Netherlands, September 2018.

8. Tuinstra, M., Olsen, H., and van Oosten, N., "NOISE: Final Report," EASA final report, European Union Aviation Safety Agency, April 2024.

9. Gopalan, G., *Quasi–Static Acoustic Mapping Of Helicopter Blade-Vortex Interaction Noise*, Ph.D. thesis, University of Maryland, 2004.

10. Schmitz, F. H., "Reduction of Blade-Vortex Interaction (BVI) Noise through X-Force Control," *Journal of the American Helicopter Society*, Vol. 43, (1), 1998, pp. 14–24. DOI: 10.4050/JAHS.43.14.

11. Greenwood, E., and Rau, R., "A Maneuvering Flight Noise Model for Helicopter Mission Planning," *Journal of the American Helicopter Society*, Vol. 65, 2020, pp. 1–10. DOI: 10.4050/JAHS.65.022007.

12. Lopes, L., and Burley, C., "ANOPP2 User's Manual: Version 1.2," NASA TM 2016-219342, National Aeronautics and Space Administration, 2016.

13. Stephenson, J. H., Pascioni, K. A., Houston, M. L., Stutz, C. M., and Martin, P. B., "Overview of a Comprehensive MD530F Acoustic Flight Test," Vertical Flight Society's 81st Annual Forum & Technology Display, Virginia Beach, VA, May 2025. DOI: 10.4050/F-0081-2025-24.

14. Society of Automotive Engineers, "Aerospace Recommended Practice (ARP) - Standard Values of Atmospheric Absorption as a Function of Temperature and Humidity," Technical Report ARP-886A, SAE, 1975. DOI: 10.4271/ARP866A.

15. Zorumski, W. E., "Aircraft Noise Prediction Program Theoretical Manual," NASA TM 83199, NASA, 1982.

16. Acoustical Society of America, "American National Standard Method for the Calculation of the Absorption of Sound by the Atmosphere," Technical Report S1.26-1978, ANSI, June 1978.

17. Zuckerwar, A. J., and Meredith, R. W., "Low-Frequency Sound Absorption Measurements in Air," Technical Report NASA Reference Publication 1128, NASA, Langley Research Center, Hampton, VA., November 1984.

18. Acoustical Society of America, "American National Standard Method for the Calculation of the Absorption of Sound by the Atmosphere," Technical Report S1.26-2014, ANSI, 2014.

19. Chien, C., and Soroka, W., "Sound Propagation Along an Impedance Plane," *Journal of Sound and Vibration*, Vol. 43, (1), 1975, pp. 9–20. DOI: 10.1016/0022-460X(75)90200-X.

20. Attenborough, K., "Acoustical Impedance Models for Outdoor Ground Surfaces," *Journal of Sound and Vibration*, Vol. 99, (4), 1985, pp. 521–544. DOI: 10.1016/0022-460X(85)90538-3.

21. Stutz, C. M., Stephenson, J. H., Pascioni, K. A., and Houston, M. L., "Acoustic Assessment of an MD530F Helicopter in Maneuvering Flight," Vertical Flight Society's 81st Annual Forum & Technology Display, Virginia Beach, VA, May 2025. DOI: 10.4050/F-0081-2025-66.

22. Akima, H., "A New Method of Interpolation and Smooth Curve Fitting Based on Local Procedures," *Journal of the ACM (JACM)*, Vol. 17, (4), 1970, pp. 589–602. DOI: 10.1145/321607.321609.

23. Spiegel, P., Buchholz, H., and Pott-Pollenske, M., "Highly Instrumented BO105 and EC135-FHS Aeroacoustic Flight Tests Including Maneuver Flights," Paper 1, Proceedings of the 61^{st} Annual Forum of the American Helicopter Society, Grapevine, TX, June 2005.

24. Guntzer, F., Spiegel, P., and Lummer, M., "Genetic Optimizations of EC-135 Noise Abatement Flight Procedures Using an Aeroacoustic Database," Proceedings of the 35^{th} European Rotorcraft Forum, Hamburg, Germany, September 2009.